Clim. Past Discuss., 11, 2341–2388, 2015
www.clim-past-discuss.net/11/2341/2015/
doi:10.5194/cpd-11-2341-2015

Climate of the Past Discussions
Open Access

Spatial and temporal oxygen isotope variability in northern Greenland – implications for a new climate record over the past millennium

S. Weißbach[1], A. Wegner[1], T. Opel[2], H. Oerter[1], B. M. Vinther[3], and S. Kipfstuhl[1]

[1]Alfred Wegener Institut Helmholtz-Zentrum für Polar- und Meeresforschung, Bremerhaven, Germany
[2]Alfred Wegener Institut Helmholtz-Zentrum für Polar- und Meeresforschung, Potsdam, Germany
[3]Centre for Ice and Climate, Niels Bohr Institute, University of Copenhagen, Denmark

Received: 07 May 2015 – Accepted: 02 June 2015 – Published: 23 June 2015

Correspondence to: S. Weißbach (stefanie.weissbach@awi.de)

Published by Copernicus Publications on behalf of the European Geosciences Union.

Abstract

We present for the first time all 12 δ^{18}O records obtained from ice cores drilled in the framework of the North Greenland Traverse (NGT) between 1993 and 1995 in northern Greenland between 74 to 80° N, 36 to 49° W and 2000 to 3200 m a.s.l. The cores cover an area of 680 km × 317 km, ~ 200 000 km^2 or 10 % of the area of Greenland. Depending on core length (100–175 m) and accumulation rate (90–200 kg m^{-2} a^{-1}) the records reflect an isotope-temperature history over the last 500–1100 years.

The δ^{18}O signal in northern Greenland is influenced by temperature, accumulation and the topography of the North Greenland ice sheet between 72 and 80° N. About 12 % of the variability can be attributed to the position of the single drill sites in relation to the ice sheet topography.

Lowest δ^{18}O mean values occur north of summit and east of the main divide. In general, ice cores drilled on the main ice divide show different results than those drilled east of the main ice divide that might be influenced by secondary regional moisture sources.

A stack of all 12 NGT records and the NGRIP record is presented with improved signal-to-noise ratio. This stack represents the mean δ^{18}O signal for northern Greenland that is interpreted as proxy for temperature. Our northern Greenland δ^{18}O stack indicates isotopically enriched periods compared to their average during medieval times, about 1420 ± 20 AD and from 1870 AD onwards. The period between 1420 AD and 1850 AD was isotopically depleted compared to the average for the entire millennium and represents the Little Ice Age. The 20th century has isotopic values higher than the 1000 years mean and is comparable to the medieval period but lower than about 1420 AD.

CPD
11, 2341–2388, 2015

1 Introduction

During the past decades the Arctic region has experienced a pronounced warming exceeding that of other regions (e.g. Masson-Delmotte et al., 2015). To set this warming into an historical context, a profound understanding of natural variability of past climate of the Arctic is essential. To do so, studying climate records is the first step. However, meteorological measurements in the Arctic are only available for relatively short time periods; only a few time series start already in the 19th century. Hence, proxy data from climate archives such as ice cores from the polar ice caps are necessary.

Studying the climate of the past centuries allows us to compare the instrumental data with proxy records and therefore to assess the quality of the proxies for climate reconstructions.

Stable water isotopes (here δ^{18}O) in ice cores are used to derive paleo-temperatures (e.g. Fischer et al., 1998c; Johnsen et al., 2000; Steffensen et al., 2008). They are largely controlled by equilibrium and kinetic fractionation processes during evaporation at the ocean surface, along the poleward air-mass transport and condensation of precipitation, depending on temperature and moisture conditions (Dansgaard et al., 1969).

The isotope ratio is not only driven by local temperature, but is affected by several factors like moisture sources and their proximity to the deposition site, the topography of the ice sheet and the seasonality of precipitation. In addition the isotope signal is altered by post-depositional processes like wind-induced redistribution of snow, temperature gradient metamorphism and diffusion. Stacked records are used to compensate for effects due to regional differences and to improve the signal-to-noise ratio (Fisher et al., 1985).

To date, most ice core studies on the Greenland ice sheet were carried out point wise (e.g. Dye 3, GRIP, GISP2, NGRIP), which poses the question: how representative is one single long ice core record to derive a record of past climate? A study of ice cores from southern Greenland revealed that winter season stable water isotopes are

CPD
11, 2341–2388, 2015

influenced by the North Atlantic Oscillation (NAO) and are strongly related to southwest Greenland air temperatures. On the other hand, summer season stable water isotope ratios show higher correlations with North Atlantic sea surface temperature conditions (Vinther et al., 2010). In particular, northern Greenland has been little investigated so far, even though it differs significantly from the south in terms of lower air temperatures and lower snow accumulation rates (Fischer et al., 1998c). Thus, the results from southern Greenland are not directly transferable to the northern part. For a correct estimate of mass balances as well as the response to the ongoing climate change, knowledge of accumulation rates and the spatial distribution of δ^{18}O as a temperature proxy are important for the entire Greenland ice sheet. However, due to northern Greenland's remoteness its recent past climate has, up to now, only been little investigated.

Using the accumulation rates of the updated (compared to Friedmann et al., 1995; Schwager, 2000) Alfred-Wegener Institute (AWI) North-Greenland-Traverse (NGT) data, it was possible to show that the area of lower accumulation rates is much larger than expected before, which has a huge influence on the outlet glaciers (Weißbach et al., 2015).

The NGT ice cores offer for the first time the possibility to study the spatial and temporal variability of stable oxygen isotope records from northern Greenland. Furthermore, they allow the analysis of the common spatial stable water isotope signal in northern Greenland by stacking the individual records to significantly reduce the isotopic noise that is present in a single data record due to local peculiarities.

The main objectives of this study are (1) to investigate the spatial variability of δ^{18}O in northern Greenland using this new set of δ^{18}O data and to evaluate the influence of isotopic noise on a single record, (2) to assess whether stable water isotope records from sites with low accumulation rates can be interpreted as climate signals, (3) to present a new robust stacked δ^{18}O record for northern Greenland covering the past millennium, and (4) to interpret this record in terms of paleoclimate with respect to temporal variability and relation to large-scale climate information from other proxy records.

CPD
11, 2341–2388, 2015

2 Material and methods

The ice cores presented here were drilled during the NGT from 1993 to 1995. In total, 13 ice cores (B16–B23, B26–B30) from 12 different sites (Table 1, Fig. 1) were drilled along the traverse route. The ice cores cover the last 500–1000 years. The drillings were accompanied by extensive surface snow studies (e.g. Schwager, 1999).

B21 and B23 as well as B26 to B30 are located on ice divides (Fig. 1) while B16–B20 were drilled east of the main ice divide. The NGRIP core (North Greenland Ice Core Project Members, 2004) was drilled 14.5 km northwest of B30 following the main ice divide and is therefore included in this study.

Before analyzing the stable water isotopes, a density profile of each core was measured. To do so, the single core segments (approximately 1 m long) were weighed in the field. Additional higher-depth resolution density records were determined using gamma-absorption measurements in the AWI cold lab (Wilhelms, 1996). Finally, in 2012 density of the first 70 m of the three cores B19, B22 and B30 was analysed by X-ray computer tomography (X-CT, Freitag et al., 2013).

An exponential function fitted to the data taking into account all three types of density data with same respect was used to calculate water equivalent (w. eq.) accumulation rates and to synchronize the cores.

Selected parts of B30 were also analyzed for electrolytic conductivity using high resolution continuous flow analysis.

For the isotopic measurements the ice was cut in samples of 1–5 cm depth resolution, corresponding to 2–10 samples year^{-1}. After melting δ^{18}O was determined using mass spectrometers type Delta E und S from Finnigan MAT in the AWI laboratory with uncertainties less than 0.1 ‰ as determined from long-term measurements. The cores B27 and B28 were drilled at the same site. Parts of the core B27 (8.25–11.38 m water equivalent, w. eq.), corresponding to AD 1926–1945) got lost, and were replaced by the record from B28. For the other parts, the mean of both dated cores was calculated to generate one isotope record for this site.

CPD
11, 2341–2388, 2015

Six of the NGT cores (B16, B18, B20, B21, B26 and B29) were already dated up to a certain depth by annual layer counting (using density, major ions or $\delta^{18}O$) in prior studies (e.g. Fischer and Mieding, 2005; Fischer et al., 1998a, b; Schwager, 2000). Depending on the availability of data and differences in snow accumulation rates the dating quality of these cores varies between 1 and 5 years accuracy. For the other NGT cores annual layer counting was not possible due to the very low accumulation rates. To achieve the same dating quality for all NGT cores for better comparison and to apply the dating on the whole core length, we used a new dating procedure for all cores. From density corrected (w. eq.) high resolution electrical conductivity profiles (Werner, 1995; Wilhelms, 1996) and SO_4^{2-}-concentration profiles for B16, B18, B21 (Fischer et al., 1998a, b), B20 (Bigler et al., 2002) and electrolytic conductivity profile (B30), distinct volcanic horizons were identified and used as match points to synchronize the cores (Table 2). Some of the volcanic eruptions show a more pronounced signal in the Greenlandic ice than others. Thus not all eruptions could be identified in every record.

Between match points, the annual dating was assigned assuming a constant snow accumulation rate. If a volcanic match point could not be clearly identified in an ice core, the next time marker was used to calculate the mean accumulation rate. Below the deepest volcanic match point, the last calculated accumulation rate was extrapolated until the end of the core.

3 Results

3.1 Depth-age models and snow accumulation rates

The last millennium was a volcanically active time (Sigl et al., 2013). The volcanic aerosols deposited on the Greenland ice sheet can be used as time markers. The depths of peaks in conductivity and sulfate concentration attributed to certain volcanic horizons are given in Table 2 as used for our dating approach.

CPD
11, 2341–2388, 2015

During the last 500 years, the time period between two detectable eruptions at NGT sites does not exceed 100 years for all the cores. This leads to a dating uncertainty for each core smaller than 10 years compared to the annually counted timescales (Mieding, 2005; Schwager, 2000), minimal at the matching points. The three youngest volcanic reference horizons (Katmai, Tambora and Laki), the eruption from 1257 AD (Samalas), and 934 (Eldgia) were found in all cores, whereas the other eruptions could not be clearly identified in every ice core. We could not find a common pattern (e.g. distance, strength of the eruption) whether or not horizons could be observed in all records.

This already indicates a high spatial variability within the study region related to significant influences of local to regional peculiarities (e.g. wind drift or sastrugi formation). An overview of the resulting mean accumulation rates for the entire core lengths for all NGT drilling sites as well as the respective ranges are given in Table 3. According to our dating, the cores reaching furthest back in time are B18, B19 and B20, covering more than the last 1000 years. These northeasterly cores have the lowest accumulation rates with values below 100 $kg\,m^{-2}\,a^{-1}$ (B19: 94 $kg\,m^{-2}\,a^{-1}$, B20: 98 $kg\,m^{-2}\,a^{-1}$), whereas the highest mean accumulation rate is found for B27/28 in the southwest of our study region with 180 $kg\,m^{-2}\,a^{-1}$. Generally, the accumulation rate decreases from the sites located on the main ice divide in the south west of the study area to the north east.

The observed range of accumulation at one single site is highest for the southwestern cores (B30 and B29) ranging between 137 and 161 $kg\,m^{-2}\,a^{-1}$ (B29). Lowest values are found for the cores east of the main ice divide (e.g. B17, B18 and B19) ranging between 113 and 119 $kg\,m^{-2}\,a^{-1}$ (B17).

3.2 Spatial variability of $\delta^{18}O$ in northern Greenland

Annual mean $\delta^{18}O$ records of the NGT cores are displayed in Fig. 2. Table 4 summarizes the main $\delta^{18}O$ characteristics of each core.

CPD
11, 2341–2388, 2015

The length of the records varies depending on accumulation rate and total length of the core. The longest records are from B19 (back to 753 AD) and B20 (back to 775 AD). The following comparisons of the individual records refer to the longest common time window (1505–1953 AD). Although diffusion is known to change isotopic values in the snow, in this study the data were not corrected for diffusion effects because the very low accumulation rates would hamper this calculation.

The lowest mean values (B16–B18) are found east of the main ice divide and north of the summit, but not at the summit as might be expected. Generally, the cores located east of the main ice divide show lower mean δ^{18}O values than those located on the ice divide (Fig. 3a). For instance, B30, and B29 are on similar altitude and latitudes as B16 and B17 but show significantly heavier values (Fig. 3a).

The maximum difference in mean δ^{18}O values of individual ice cores is 3.3 ‰ (highest mean δ^{18}O in B26: −33.86 ‰, lowest mean δ^{18}O in B17: −37.13 ‰). The standard deviation (SD) within each core in the common time window (1505–1953 AD) is lowest for B16 (0.99 ‰) and highest for B18 (1.44 ‰). We found no general relation between accumulation rate and standard deviation of the δ^{18}O values for all individual cores, even though the northern cores with generally lower accumulation rates show higher standard deviations than the southern cores.

In Fig. 2, we compare our individual NGT δ^{18}O records to other published Central to North Greenland (GRIP, GISP2, NGRIP) δ^{18}O time series. Prominent decadal-scale maxima and minima occurred mostly isochronally. However, specific events such as warm periods around 1420 AD or 1920–1930 AD or a cold period in the 17th century are more pronounced in the NGT cores compared to summit.

Some records show faster changes between warmer and colder events (e.g. GRIP, B30 and B26), while others (e.g. B17–B21) remain longer at values higher or lower than their mean (Fig. 2). The longest warm period (compared to the mean of whole core length) is found in B19 (with 37 subsequent years warmer than the mean), while B17 has the longest cold period (28 subsequent years colder than mean). GRIP, B26, and B27/28 show a higher frequency with a maximum of about ten subsequent warmer

CPD
11, 2341–2388, 2015

or colder years. In general, the first half of the last millennium was characterized by longer warm or cold anomalies than the second half.

We investigated the relationship between the altitude, latitude and longitude of the drilling sites and the mean δ^{18}O values (Fig. 4a–c), which are statistically significant ($p < 0.05$) only for longitude and latitude. Among the factors influencing the mean isotopic composition, the longitude has the strongest impact ($R^2 = 0.56$). Figure 4c shows the clear east-to-west gradient in the mean δ^{18}O values in northern Greenland. In contrast, the effect of the altitude is rather low ($R^2 = 0.13$) and not statistically significant.

From the regression functions, we find that in northern Greenland δ^{18}O values decrease from north to south and west to east as well as from higher to lower altitudes (Fig. 4).

Regarding snow accumulation rate we differentiate two groups: (I) cores with accumulation rates lower than 145 kg m^{-2} a^{-1} mainly located east of the main ice divide (B16–B21 and B23) and (II) cores with higher accumulation rates (B22, B26–B30 and NGRIP). We find heavier δ^{18}O ratios for sites with higher accumulation rates (Fig. 4d). The relationship is weak but becomes stronger for higher accumulation rates.

The correlation coefficients between the annual δ^{18}O-records of individual ice cores are relatively small ($r = 0.1$ to 0.36, $p < 0.05$). This can be partly explained by the fact that the 13 northern Greenland (NG) drilling sites (12 NGT and NGRIP) are up to 680 km apart from each other. The strongest correlations are found for the cores from the southwest (B30–B26) and the lowest for those from the northeast (B19, B20). There is a significant linear relationship between the distance between the core sites and their annual δ^{18}O correlation coefficient ($r = -0.44$, $p < 0.05$). However, it is not always true that the cores with smallest distance between them have the highest correlations.

For smoothed values (5 year running mean) the correlation coefficients between the δ^{18}O records are only slightly higher. Only 25 % of the combinations have coefficients higher than 0.3, and 15 % are lower than 0.1. This indicates an important influence of regional site to site differences.

CPD
11, 2341–2388, 2015

To study the regional-scale patterns of common variability of all annual δ^{18}O records, we performed a principal component analysis (PCA). All calculations are done for the largest common time window of all cores (1505–1953 AD). Other time periods were used as well, and they show similar results.

Only the first two principal components (PC1 and PC2) are above the noise level. The first two eigenvectors of the isotopic time series explain 34.1 % of the total variance (PC1: 21.8 %, PC2: 12.3 %). The other PCs are dominant in one or two records but are not significant for the total variance of the entire dataset. The loading patterns are mapped in Fig. 5 and show a homogeneus pattern for PC1 and a bipolar result for PC2.

3.3 The northern Greenland δ^{18}O-stack

To reduce the noise in the single δ^{18}O records, we calculated a stacked record by averaging the 13 annual NG δ^{18}O records in their overlapping time periods (Fig. 6). Before stacking, all records were centred and normalized regarding their common time window (1505–1953 AD). The SD of the NG-stack (0.44 for 1505–1953 AD) is less than half of the SD in annual δ^{18}O records of the individual cores. Also Vinther et al. (2010) make clear that stacking is important to improve signal-to-noise ratio in low accumulation rate areas. Local drift noise would account for half of the total variance in single-site annual series (Fisher et al., 1985).

As the NG-stack before 1000 AD is based on only four records (< 25 % of the total core numbers), we decided to focus in the following only on the time period after 1000 AD.

To investigate the relationship of the NG-stack with air temperature, we used monthly meteorological observations from coastal southwest Greenland sites and Stykkisholmur in Northwest Iceland available from the Danish Meteorological Institute (DMI – http://www.dmi.dk; 1784–1993 AD) and the Icelandic Meteorological Office (http://en.vedur.is/; back to 1830 AD), respectively. We selected only the Greenlandic tem-

CPD
11, 2341–2388, 2015

perature records longer than 200 years for our study even though they are in large distance (706–2206 km).

The correlation coefficients between the NG-stack and these air temperature records are shown in Table 5. Dating uncertainties are taken into account by comparing 5 year running means. The NG-stack shows low but significant ($p < 0.001$) correlations to the air temperatures at all sites (Table 5).

The strongest correlation with annual mean temperature was found for the merged station data at Greenland's southeast coast ($r = 0.51$), and the temperature reconstruction for the North Atlantic Arctic boundary region of Wood et al. (2010) ($r = 0.55$); the lowest was found for Qaqortoq ($r = 0.39$) also in the south of Greenland (Table 5). For Stykkisholmur the correlation is in the range of the Greenlandic ones ($r = 0.41$). Slightly higher correlations are obtained by comparing the NG-stack to seasonal data. Except for Ilulissat, winter months (DJF) show weaker correlations; spring (MAM) and summer (JJA) months show stronger correlations to the NG-stack.

Although the NG-stack record shows some correlation with temperature data from coastal Greenland sites, it remains an open question, how the NG-stack $\delta^{18}O$ variations can be converted to absolute temperature changes within North–East Greenland during the last millennium.

For more than 30 years such conversion of isotopic time series of Greenland ice cores was based on a modern analogue approach taking the observed spatial isotope/temperature gradient of 0.67 ± -0.2 ‰ $^{\circ}C^{-1}$ (Dansgaard, 1964; Johnsen et al., 1989) as a valid calibration for converting isotope records of Greenland ice cores into temperature changes (e.g. Grootes et al., 1993). The strong confidence of glaciologists into this approach came principally from two observations. (1) Over both polar ice sheets, the spatial correlation between modern isotope and annual mean temperature is very high and significant. (2) This empirical observation was theoretically understood as a consequence of a Rayleigh rainout system controlling the isotopic composition of meteoric water.

CPD
11, 2341–2388, 2015

However, for the Greenland area this long time accepted approach has been challenged during the last decade. Two entirely independent analytic techniques, one based on the numerical interpretation of borehole temperatures (e.g. Dahl-Jensen et al., 1998) and the other based on the occlusion process of gases into the ice (e.g. Buizert et al., 2014; Severinghaus et al., 1998) allow a direct temperature reconstruction at least for some periods of the past. Consistently both methods point to much lower temporal δ^{18}O T^{-1} slopes ranging between 0.4–0.3 ‰ °C^{-1} (Jouzel et al., 1997a). Consequently they indicate a much higher temperature variability in Greenland during the last glacial period. For the period of the last 9000 years the Greenland average Holocene isotope–temperature relationship has been estimated to be 0.44–0.53 ‰ °C^{-1} again substantially lower as the modern spatial gradient (Vinther et al., 2009). However, as all these studies cover much longer time periods as compared to our NG-stack records, no firn conclusion can be drawn from these studies about an appropriate isotope–temperature relationship for the last millennium.

Along the NGT firn temperature measurements in about 15 m depth had been done. But due to their small range of about 2 K difference it is difficult to reassess the general Greenland isotope temperature relationship from Johnsen et al. (1989) from the NGT data, solely. Schwager (2000) added data from Dansgaard et al. (1969) from along the EGIG traverse, which was also used in Johnsen et al. (1989), to expand the temperatures range to derive a more reliable isotope-temperature gradient. This calculated gradient of 0.7 ± −0.2 ‰ °C^{-1} is within the gradient uncertainty range given by Johnsen et al. (1989). Using our updated NGT dataset we get the same results.

If we apply the spatial isotope/temperature gradient of 0.7 ‰ °C^{-1} for the range of isotope variations (−1.43 to 2.51 ‰) of the NG-stack record, the isotope data would translate into temperature changes of −2.04 to 3.59 °C within the last millennium. However, applying instead a temporal gradient of 0.48 ‰ °C^{-1} as suggested by Vinther et al. (2009) results in possible temperature changes of −2.98 to 5.23 °C within the last 1000 years. Using the most recent temporal glacial–interglacial isotope-temperature

CPD
11, 2341–2388, 2015

gradients reported by Buizert et al. (2014) would result in comparable temperature changes.

The resulting temperature ranges are larger than expected (e.g. Dahl-Jensen et al., 1998) which is an additional argument not to calculate absolute temperatures from the NG-stack with the given gradients.

We conclude that any conversion of the NG-stack isotope record into absolute temperature variations during the last millennium is highly uncertain. Thus, for the following part of the manuscript, we will refer to NG-stack isotope anomalies as relative temperature changes in terms of "warmer" (i.e. isotopically enriched) and "colder" (isotopically depleted), only, but refrain from converting our ice core data into absolute temperature changes.

3.4 Last millennium climate from stacked NG δ^{18}O record

The NG-stack covers the time between 753 AD and 1994 AD (Fig. 6). For a better visualisation of decadal to centennial scale variability a 30 year running mean is added. The running mean shows the warmest period around 1420 AD and the coldest in 1680 AD. The isotopically warmest single year during the last 1000 years in northern Greenland was 1928 AD, whereas 1835 AD was the coldest.

Distinct decadal- to centennial-scale warm and cold anomalies can be detected in the stacked (Fig. 6) as well as individual δ^{18}O records (Fig. 2) and are partly related to well-known climate anomalies such as the Medieval Climate Anomaly (MCA, 950–1250 AD, Mann et al., 2009), the Little Ice Age (LIA, 1400–1700 AD, Mann et al., 2009) and Early Twentieth Century Warming (ETCW 1920–1940 AD, Semenov and Latif, 2012).

We find a pronounced warm period from 850 to 1100 AD, which has its maximum between 900 and 1000 AD. This is about 100 years earlier than the described MCA in Mann et al. (2009). The warm period is followed by a quasi-periodical change of warm and cold phases observed approximately every 50 to 70 years until about 1600 AD. During this phase, the most distinct warm period is observed around 1420 AD.

CPD
11, 2341–2388, 2015

A longer period of cold temperatures occurred during the 17th and early 19th century and was already attributed to the LIA by a prior NGT study that used only 4 cores (B16, B18, B21 and B29, Fischer et al., 1998c). A cold period in northern Greenland corresponding to the LIA is later than reconstructed for the Northern Hemisphere by Mann et al. (2009), with lowest values during 1620–1780 AD and in the first half of the 19th century. Interestingly, the warmest mean values of the last 1000 years at 1420 AD lie within the timeframe of LIA.

A clear, but compared to other periods not outstanding, warm event corresponding to the ETCW is in the early 20th century. Since the 1870s AD, the values are above the 1000 year mean. At the end of the 20th century, the temperature stagnates at a high mean level. However, as the NGT cores were drilled between 1993 and 1995 AD, the warmest years of the recent decades (Wood et al., 2010) are not included in our record.

For the NG-stack as well as most of the individual NGT cores the isotopically warmest periods besides the 1420 AD event were in the 10th and 20th centuries, in particular between 1900 and 1950 AD. These years are even warmer than the most recent years covered by the NGT cores (i.e. the 1980s).

4 Discussion

4.1 Regional δ^{18}O variability in northern Greenland

Stable water isotope ratios in ice are widely used as a proxy for air temperature (Dansgaard, 1964; Johnsen et al., 1995; Jouzel et al., 1997b). In this section, we will discuss the representativity of a single ice core δ^{18}O-record in northern Greenland and the influence of different aspects as changes in altitude, latitude, longitude or accumulation rate on the stable water isotope ratio. The comparison to direct air-temperature observation data and proxy data allows to assess the quality of the proxy in terms of paleo-climatological interpretation.

CPD
11, 2341–2388, 2015

4.1.1 Spatial distribution

Variability in $\delta^{18}O$ is dependent on local (e.g. wind), regional (e.g. position on the ice sheet) and large-scale (e.g. circulation patterns) processes. Even adjacent cores may differ considerably according to snow drift (Fisher et al., 1985). In this study, and as expected from the large distances between the drilling sites, correlations between the $\delta^{18}O$-records are generally relatively low ($r < 0.36$ for annual values). One further reason for the lower correlations may be attributed to dating uncertainties. As smoothing the data does not increase the correlation coefficient significantly (still $r < 0.5$ for 5 year running mean values), we conclude that different regional influences on the $\delta^{18}O$ values play a more important role. All cores with the higher correlations (B23, B26, B27/28, B29 and B30) are located in the same area in the western part of northern Greenland whereas all other cores are located more to the east.

The PC1 has negative loadings on all the time series and therefore represents a homogenous regional-scale pattern even though the loadings for the cores on the ice divide are higher. In contrast, PC2, as the second strongest influence, shows a pronounced east–west difference (Fig. 5). A similar pattern with distinct differences between the main ice divide region and the eastern region can also be found in several other aspects.

We found lighter $\delta^{18}O$ values in the southern and eastern part of northern Greenland in contrast to the general speculations of Dansgaard (1954), who expected lighter values northward. The east-to-west difference is also expressed by the dependency of $\delta^{18}O$ values on longitude (Fig. 4). This is in line with results from Box (2002), who found that there is often an opposite trend in air temperatures in east and west Greenland. The antiphase of temperature records from east and west Greenland is may be explained by the importance of different weather regimes (e.g. Ortega et al., 2014).

The range in $\delta^{18}O$ in the different cores is different, too. Cores drilled in the northeast that are characterized by the lowest accumulation rates have the highest standard

CPD
11, 2341–2388, 2015

deviations (SD) in δ^{18}O, which can be partly explained by the fact that a smaller number of accumulation events scatters easier.

The east-to-west difference is also detectable in the temporal variability of the annual δ^{18}O values. Cores with more rapid fluctuations are from summit and the main ice divide, while those cores drilled east of the divide have longer periods of positive or negative anomalies. We conclude that east of the divide, the climate conditions are not as variable and therefore the annual δ^{18}O signal is of greater persistence.

Taking all these aspects together, we argue that the main ice divide has a large influence on the spatial δ^{18}O pattern representing temperatures.

The main ice divide separates the Greenland ice sheet into eastern and western regions (Fig. 1). Cyclonic activity is most important for the precipitation over Greenland. Cyclones forming over Hudson Bay or Baffin Bay and winds from the west or southwest transport air masses to Greenland (Chen et al., 1997). The cyclonic influence decreases from south to north and from west to east because of the blocking influence of the summit and the main ice divide. Furthermore, we observe a stronger isotope–altitude relationship for the cores on the ice divide ($r = 0.96$). This may be explained by different atmospheric circulation conditions allowing additional moisture from other sources to reach the region east of the ice divide. This is supported by the finding of Friedmann et al. (1995) which suppose based on data from B16 to B19 that northeast Greenland receives more moisture from local sources as the Greenlandic Sea, Atlantic Ocean and the Canadian Wetland, in particular during summer.

Buchardt et al. (2012) noted that the relationship between accumulation rate and δ^{18}O is not distinct for Greenland. They see the "foehn effect" (dry warm wind in the lee of the ice divide) as one reason. The foehn effect causes an anticorrelation between δ^{18}O and accumulation rate, which is not seen in central Greenland but on the lee side east of the ice divide in southern Greenland, as also visible for our data in Fig. 4d. Furthermore Buchardt et al. (2012) find that the sensitivity of δ^{18}O changes in accumulation rate is smallest in northeast Greenland (North Central and North, 1972), which is in agreement with our findings.

CPD
11, 2341–2388, 2015

B16, B17 and B18 have the lowest mean δ^{18}O values (about −37 ‰) observed so far in northern Greenland and maybe also the lowest in Greenland. This is in contrast to the findings of Ohmura (1987), who suggested for this region temperatures similar to summit. Figure 4 indicates that accumulation, latitude and altitude may have minor impact on the δ^{18}O values here. One possible explanation would be additional moisture isotopically depleted during the transport from rather northern directions.

The cores more to the north (B19–B22) were drilled at lower altitude and therefore record different climate signals (i.e. from lower air masses) compared to the high altitude ice cores that, in turn, record a more smoothed signal of higher atmospheric layers. Similar effects were observed e.g. in Svalbard (Isaksson et al., 2005), even though in considerably lower altitudes compared to Greenland.

Johnsen et al. (1989) found a regression slope of δ^{18}O with respect to latitude $\delta(\delta^{18}\mathrm{O})/\delta\,(\text{latitude}) = -0.54\,‰\,\text{degree}^{-1}$ and with respect to altitude $\delta(\delta^{18}\mathrm{O})/\delta\,(\text{altitude}) = -0.006\,‰\,\text{m}^{-1}$ for large areas of Greenland.

The multiple linear regressions show enormous uncertainties of the elevation and latitude relationship. Using the parameters given by Johnsen et al. (1989), it is not possible to calculate certain δ^{18}O relationships to altitude and geographic position from northern Greenland's ice cores. However, using different tuning factors for the Johnsen model, it was possible to accomplish almost equal R^2 (~ 0.8) for northern Greenland's δ^{18}O values compared to the Johnsen et al. (1989) results. Applying this approach to our data, we find $\delta(\delta^{18}\mathrm{O})/(\delta\,(\text{latitude}) = -0.30\ (\pm 0.40)\,‰\,\text{degree}^{-1}$ and $\delta(\delta^{18}\mathrm{O})/\delta\,(\text{altitude}) = -0.0035\ (\pm 0.0024)\,‰\,\text{m}^{-1}$. The regression residuals are linearly related to longitude as well as accumulation rate (Fig. 7).

This justifies that for northern Greenland ice cores, the differences in mean δ^{18}O can be largely explained by geographic gradients in topography (i.e. altitude, latitude and longitude) and accumulation rate. Thus, we assume that the variability in the NG stacked δ^{18}O record represents past temperature development.

We assume air temperature to be the main influence (PC1) on the δ^{18}O values. There is a strong correlation of the PC1 (northern Greenland δ^{18}O values) to the NG-

CPD
11, 2341–2388, 2015

stack ($r = -0.97$, $p \ll 0.01$). This leads to the conclusion that 22 % of the signal in the northern Greenland δ^{18}O records can be interpreted as a regional climate signal. This is supported by the fact that Vinther et al. (2010) found for their PC1 from winter δ^{18}O values from southern Greenland's ice cores a strong correlation ($r = 0.71$) to air temperature data.

The main divide influences the pathways of air masses, causing the "foehn effect" and thus lower accumulation rates in the east. Thus we conclude that the largest part of the spatial differences in δ^{18}O values in northern Greenland is caused by the influence the topography of the ice sheet on the regional climate system.

4.1.2 Paleoclimatic significance of the stacked δ^{18}O

As the NG-stack is a result of 13 ice cores over a large area we assume its regional representativity. From the PCA we know that the first two PC's are significantly correlated to the NG-stack, which supports the validity of the stack.

A direct comparison of the δ^{18}O and direct air temperature measurements is hindered by the distance between drill sites and weather stations and results in relatively low correlations (Table 5). Comparably low correlations between annual δ^{18}O means and measured temperatures from coastal stations are also reported for the NEEM record (Steen-Larsen et al., 2011).

However, the rather low correlation coefficients might underestimate the real regional δ^{18}O-temperature relations because of different reasons.

We expect that the most important reasons are the large distances and the difference in altitude (i.e. more than 2000 m) between drill sites and the meteorological stations, which let them receive different atmospheric signals. The stations are located at the coast and are in turn also likely influenced by local factors as the occurrence of sea ice. The difference in altitude is also one important fact causing the differences in GRIP and DYE3 borehole temperature data (Dahl-Jensen et al., 1998).

One other aspect might be the seasonality as argued by Steen-Larsen et al. (2011) for the NEEM site. The snow fall in northern Greenland may be seasonally unevenly

CPD
11, 2341–2388, 2015

distributed. However, it is not possible to generate sub-annual data for northern Greenland ice cores due to low accumulation. We find a tendency to stronger correlation between the annual $\delta^{18}O$ and summer (JJA, r = 0.35–0.51) and spring (MAM, r = 0.36–0.62) temperatures for most of the stations. This points to a higher proportion of summer snow in the annual accumulation in northern Greenland, too.

Also regional noise factors such as wind drift and sastrugi formation as well as uncertainties in ice core dating and the usage of very old observation data have to be taken into account.

In summary, we consider the northern Greenland $\delta^{18}O$ stacked record as a reliable proxy for annual temperature for northern Greenland. The regional representativeness of the NG-stack is supported by the general similarity to the NEEM $\delta^{18}O$ record (Masson-Delmotte et al., 2015) for the period 1724–1994 AD. Even single events such as the highest values in 1928 AD and the 1810–1830 AD cooling occur in both records.

To assess regional differences within northern Greenland, stacks of subsets of cores will be discussed in terms of interpretation as a temperature proxy. As illustrated in Fig. 4, we differentiate two different types of cores, cores drilled on the ice divide and cores drilled east of the ice divide. Accordingly, in Fig. 6 the overall northern Greenland $\delta^{18}O$ stack used in this study is compared to a stack of the cores of lower accumulation rate drilled east of the main ice divide (B16, B17, B18, B19, B20, B21 and B23) (group I) and a stack of those on the ice divide (B22, B26, B27, B29, B30 and NGRIP) (group II) (Fig. 8).

Even though there is a similar overall trend, the three records show differences in amplitude and timing of warm and cool events. The correlation between the two substacks is rather low (r = 0.71). In the 11th and 12th centuries, we observe a quasi-anti-correlation between group I and group II. Even during the well-known climate events (MCA, LIA, ETCW, marked in Figs. 6 and 8), there are significantly different $\delta^{18}O$ patterns. For example, group II (ice divide) shows colder temperatures during 1000–1200 AD. Also, during the 16th century we notice substantial differences between the

CPD
11, 2341–2388, 2015

two sub-stacks. In group I (east, low accumulation rate) events like the 1420 AD or the first part of the LIA show a higher amplitude.

The stack of group I (east, low accumulation rate) has a higher correlation to the total NG-stack ($r = 0.96$) compared to group II ($r = 0.67$) for the period 994–1994 AD. Looking at the time period 1505–1993 AD with a high number of cores included in both sub-stacks, the correlation coefficients to the total NG-stack are almost equal (group I: $r = 0.95$, group II: $r = 0.90$, $p < 0.1$). Here, both records reflect the mean changes in $\delta^{18}O$ for northern Greenland. Differences before 1505 AD may be artefacts of low core numbers even though regional differences in climate conditions cannot be ruled out.

We consider the NG-stack as a climate record confirms our interpretation of PC1, and displays the overall climate variation independent of local influences as topography or accumulation rate. In contrast, results from studies with only one record become uncertain, as they may be affected by a lower signal-to-noise ratio and a higher influence of other local non-climate effects.

4.2 Temporal variability of arctic $\delta^{18}O$ values and their forcing factors

To set the results in an Arctic-wide context we compare our northern Greenland temperature record (NG-stack) to ice-core records from Siberia (Akademii Nauk – AN, Opel et al., 2013), Canada (Agassiz Ice Cap – Agassiz, Vinther et al., 2008), Svalbard (Lomonosovfonna – Lomo, Divine et al., 2011) and south Greenland (Dye3, Vinther et al., 2006b) as well as a multi-proxy reconstruction of annual Arctic SAT (Arctic2k, PAGES 2k Consortium, 2013; Fig. 9) that cover our time period.

Note that some of these time series (Agassiz, Arctic2k) are also stacked records with a wider regional representativeness, whereas others are single records (Dye3, AN, Lomo), which influences the strength of correlation due to different signal-to-noise ratios. For the discussion of the temperature record, we concentrate on the smoothed values (30 year running means).

The strongest correlations to our NG-stack are found for the Agassiz and Arctic2k records ($r = 0.58$ and 0.66, respectively). For the latter, we have to consider that some

CPD
11, 2341–2388, 2015

of the NGT cores (B16, B18 and B21) are used to generate this multi-proxy record. The aim of PAGES 2k was to generate an Arctic wide representative record. In total, 59 records including 16 ice cores were used. NGT cores represent only 3 out of these 59 records. The correlation coefficient between the stacked anomalies of B16, B18 and B21 and the Arctic2k temperature is small ($r = 0.24$) so we can assume that the NGT records do not dominate the reconstruction.

We conclude that a good correlation between the NG stack and the Arctic2k record show that the temperature in northern Greenland follows in general the Arctic-wide mean temperature.

The Lomonosovfonna record is interpreted as a winter record and has only a weak correlation to the NG-stack ($r = 0.22$). More summer snow in northern Greenland compared to Lomonosovfonna could be one possible explanation for the weak correlation between both records.

On a short-term scale, there are differences in the well-known climatic events (MCA, LIA and ETWC; Fig. 9), which are reflected with different intensity in the δ^{18}O values and show spatial patterns.

The Lomonosovfonna, Akademii Nauk and Arctic2k records show significantly more enriched δ^{18}O values during the MCA. However, smaller events of abnormal warm temperatures during the MCA are observed for Agassiz and Dye3. Our NG-stack shows warmer values earlier than the MCA time period given by Mann et al. (2009). We conclude that further north in the Arctic the warm events during MCA are less pronounced or earlier in timing.

The Lomonosovfonna and Arctic2k records show a dominant cold period during the LIA from 1580 to 1870 AD. Also, our northern Greenland as well as the Agassiz and Akademii Nauk ice cores reveal distinct LIA cooling periods in contrast to the Dye3 ice core from south Greenland. Like in our NG-stack, the cooling appears in two phases and some decades later than described by Mann et al. (2009). For the NG-stack, the younger phase (1800–1850 AD) is of minor amplitude and shorter duration.

CPD
11, 2341–2388, 2015

Between 1920 and 1940 AD, there was a major warming period in the Arctic, known as ETCW and observed in all shown records here. Chylek et al. (2006) determined from meteorological data that the 1920–1930 warming was stronger than the 1995–2005 warming. For the NG-stack and Akademii Nauk record, the ETCW was warmer than the second half of the 20th century, which distinguishes them from other shown records. The ETCW is assumed to be independent of external forcing but caused by internal climate variability, in particular sea ice-atmosphere feedbacks (Wood and Overland, 2010). This let us conclude that northern Greenland may also be a good place to study forcing independent climate changes.

However, natural external forcing (i.e. insolation, solar irradiance and volcanic eruptions) is assumed to influence the temperature that can be studied from northern Greenland's ice cores.

In general, higher solar activity causes higher temperatures (as during the MCA) whereas cold periods (e.g. LIA) are dominated by lower solar activity (Ammann et al., 2007). Based on some of the NGT records (B16, B18, B21 and B29), Fischer et al. (1998c) explained most of the long-term variation in northern Greenland by changes in solar activity.

Volcanism causes strong negative radiative forcing (Robock, 2000). It is assumed that volcanic eruptions inject large quantities of sulfur-rich gases into the stratosphere and global climate can be cooled by 0.2–0.3 °C for several years after the eruption (Zielinski, 2000). Results from Crowley (2000) indicate that volcanism generally explains roughly 15–30 % of the variability in global temperatures.

Miller et al. (2012) argued that century-scale cold summer anomalies of which the LIA represents the coldest one, occur because natural forcing is either weak or, in the case of volcanism, short-lived. PAGES 2k Consortium (2013) shows that periods with strong volcanic activity correspond to a reduced mean temperature. LIA may be therefore caused by a 50 year-long episode of volcanism and kept persistently cold because of ocean feedback and a summer insolation minimum.

CPD
11, 2341–2388, 2015

To check the impact of volcanic eruptions on the temperature of northern Greenland, we compared the $\delta^{18}O$ values of the high-resolution data of the individual NGT cores as well as of the stacked record 5 years before and after major volcanic eruption (Table 2).

Not in all cases are eruptions followed by a distinct cold period. For example the Tambora eruption in 1815/16 AD or Huyanaputina in 1601 AD took place within a general cold period in northern Greenland (Fig. 2), and a possible additional cooling effect cannot be clearly attributed to the volcanic eruptions. For the Mt. St. Helens eruption in 1479 AD, we see an ongoing warming trend, whereas the 1259 AD eruption took place during an ongoing cooling. Thus the eruption cannot be the reason for the onset of the cold period. After the Katmai eruption in 1912 AD, we observe a cooling in some of the cores with higher accumulation rate (e.g. B29 and B26). The cores with the lowest accumulation rates (B17–B21) do not show any temperature response to the volcanic eruption.

Thus, there is no general direct relationship between volcanic eruptions and cooling in northern Greenland; neither in the NG-stack nor in the single $\delta^{18}O$ records. It was therefore also not possible to distinguish between equatorial and Icelandic volcanoes.

The reconstructions of Box et al. (2009) showed that volcanic cooling is concentrated in western Greenland, which is consistent with the findings from instrumental records (Box, 2002; Robock and Mao, 1995), and is largest in winter as the dynamically active season. From our dataset, we conclude as Fischer et al. (1998c) that volcanic climate forcing is limited in northern Greenland.

As Swingedouw et al. (2015) argue it also might be possible that the direct cooling response of volcanic eruptions is first to the ocean and only after years seen in the $\delta^{18}O$ values from ice cores which complicates the study of cooling after volcanic eruptions from ice core data.

Between about 1100 and 1600 AD we observe quasi-periodic (50–70 a) cold and warm anomalies in the NG-stack which is not present in the other shown Arctic records (Fig. 9).

CPD
11, 2341–2388, 2015

The Atlantic Multidecadal Oscillation, AMO, could be one possible influence causing these low-frequency oscillations. As AMO index reconstruction (Gray et al., 2004) does not cover the time between 1100 and 1600 AD, we only can speculate about an influence in that time due to the similar periodicity. For the time period 1567–1990 AD, the correlation between the NG-stack and the AMO index is weak ($r = 0.06$), which might be due to the uncertainties in historical AMO data. However, since 1800 AD we observe a higher correlation coefficient ($r = 0.66$, $p < 0.05$) implying a possible relation.

One of these warmer periods is about 1420 ± 20 AD, an abnormal warm event which is observed in our northern Greenland record and has not been pointed out in other ice core studies before. The event is observable in all nine NGT cores covering this time (Fig. 2) as well as in NGRIP but not in the temperature records from southern Greenland as the Dye3 ice core (Fig. 9). One reason here might be the specific geographical position in the North.

Furthermore, we observe a difference between the Canadian and Siberian Arctic regarding the 1420-event. Unlike the Siberian Akademii Nauk ice core, the $\delta^{18}O$ values of the Agassiz cores from Ellesmere Island also show a trend to more enriched values in that period but not as strong as in northern Greenland.

The fact that the 1420 event is not clearly noticeable in other surrounding Arctic ice cores emphasizes that this event may have occurred on a smaller regional scale. However, it seems to have been of dominant influence and is also reflected in a smaller warming for the Arctic2k record (Fig. 9).

The spatial distribution of the 1420 event in northern Greenland is mapped in Fig. 3b. The event is strongest in the upper north and shows a different pattern than the $\delta^{18}O$ anomalies of the 1920–1930 warm phase, which is also attributed to internal variability and is strongest in the northeast of Greenland.

Figure 10 shows possible forcing factors causing the 1420 AD event. According to the reconstructed total solar irradiance record of Steinhilber et al. (2009), there was no solar maximum observed for 1420 AD that could explain the warmer temperatures

CPD
11, 2341–2388, 2015

in northern Greenland. As we see no forcing anomaly, we interpret the 1420-event as caused by internal Arctic climate dynamics with a sea-ice-atmospheric feedback.

Box (2002) argued that climate variability in Greenland is linked to the Northern Oscillation (NAO), volcanism and sea ice extent. NAO (Vinther et al., 2003) is calculated to be weakly reflected ($r = -0.2$, $p < 0.01$) in the NG-stack, similar to White et al. (1997) for summit ice cores, whereas none of the single NGT records is significantly correlated ($p < 0.05$) to the NAO index. The NG-stack has an increased signal-to-noise level, which is why the correlation here might be clearer than from individual records. Also, the sub-stack of the records on the ice divide (group II) as well as those east (group I) are significantly correlated ($r = -0.19$ and -0.17, $p < 0.05$) to the NAO index. The cores east of the main ice divide are expected to be out of the major cyclonic track. We conclude that NAO is not of major importance for northern Greenland δ^{18}O values.

Around 1420 AD, an anti-correlation between sea-ice extent in the Arctic Ocean (Kinnard et al., 2011) and the δ^{18}O values is observed (Fig. 10). The sea ice in the Arctic Ocean shows a recession in this time of warm temperatures in northern Greenland. A shrunken sea ice extent would cause higher temperatures on a regional scale and would increase the amount of water vapour from local sources. Therefore, compared to distant sources, more isotopically-enriched moisture (Sime et al., 2013) may contribute to precipitation in northern Greenland, in particular east of main ice divide.

However, we do not see any direct relationship between sea-ice extent and our NG-stack during the rest of time. The used sea ice record is an Arctic-wide one, which means that the climatic events of regional extent do not have to be always reflected in the sea ice extent record. Nevertheless, also the recent NEEM δ^{18}O record from northwest Greenland, shows a generally close relationship with the Labrador Sea/Baffin Bay sea ice extent (Masson-Delmotte et al., 2015; Steen-Larsen et al., 2011).

The sea-ice extend reconstruction of Kinnard et al. (2011) is based on 69 proxy records of which 22 are δ^{18}O records. Out of these 22 δ^{18}O records 5 (NGRIP, B16, B18, B21 and B26) are used also in our NG-stack. We do not expect circular reasoning

CPD
11, 2341–2388, 2015

in the interpretation of the 1420 event because B16 and B26 do not reach the age of 1420 AD and we do not see a strong anti-correlation during any other time period.

5 Conclusions

With the full set of the NGT records, it was now for the first time possible to describe regional differences in the δ^{18}O values in northern Greenland over the last 1000 years.

Because of the ice sheet topography we see a clear east-to-west difference in northern Greenland δ^{18}O distribution. The east-to-west gradient is larger than the north-to-south gradient. We find a more pronounced persistence of warm or cold events east of the main ice divide and assume more stable climate conditions there. The eastern part is more influenced by local effects like changes in the Arctic Ocean, which has to be supported by the results of climate models. For the first, time a local warm event at 1420 ± 20 AD was pointed out. We assume an atmosphere-sea ice feedback as one possible reason for this event.

Due to the shadowing effect of the main ice divide we find the lowest accumulation rates in the northeast, whereas the lowest mean δ^{18}O values are found east of the main ice divide north of summit. The lowest δ^{18}O mean values seem to be independent of accumulation rate.

We have presented a new 1000 year stacked δ^{18}O record for northern Greenland covering 10 % of the area of Greenland. We found this NG-stack to be representative for the northern Greenland temperature.

Northern Greenland δ^{18}O represents known climatic variations of the last millennium. We see a warm MCA and can derive distinct LIA cooling from our NG-stack.

The results of single site ice-core studies are likely weakened by the finding that only 22 % of the local δ^{18}O signal is related to climate. 12 % of the variability is attributed to ice sheet topography. The remaining 66 % are therefore due to other processes.

CPD
11, 2341–2388, 2015

The solar activity and internal Arctic climate dynamics are likely the main factors influencing the temperature in northern Greenland. In contrast we could not find a general cooling effect of volcanic eruptions in our data.

Acknowledgements. Stefanie Weißbach was financed by the "Earth System Science Research School (ESSReS)", an initiative of the Helmholtz Association of German Research Centres (HGF) at the Alfred Wegener Institute (AWI), Helmholtz Centre for Polar and Marine Research.

This study contributes to the Eurasian Arctic Ice 4k project funded by Deutsche Forschungsgemeinschaft (grant OP 217/2-1 awarded to Thomas Opel).

Anna Wegner acknowledges REKLIM for funding.

Many thanks to the drill and lab team who have measured the $\delta^{18}O$ with endurance over more than 20 years. We also thank Johannes Freitag and Katja Instenberg for high resolution (CT) density measurements, Martin Rückamp for compiling the maps, Martin Werner for helpful discussions that improved the manuscript and Kirstin Meyer for proofreading.

References

Ammann, C. M., Joos, F., Schimel, D. S., Otto-Bliesner, B. L., and Tomas, R. A.: Solar influence on climate during the past millennium: results from transient simulations with the NCAR Climate System Model, P. Natl. Acad. Sci. USA, 104, 3713–3718, 2007.

Andersen, K. K., Azuma, N., Barnola, J.-M., Bigler, M., Biscaye, P., Caillon, N., Chappellaz, J., Clausen, H. B., Dahl-Jensen, D., Fischer, H., Flückiger, J., Fritzsche, D., Fujii, Y., Goto-Azuma, K., Grønvold, K., Gundestrup, N. S., Hansson, M., Huber, C., Hvidberg, C. S., Johnsen, S. J., Jonsell, U., Jouzel, J., Kipfstuhl, S., Landais, A., Leuenberger, M., Lorrain, R., Masson-Delmotte, V., Miller, H., Motoyama, H., Narita, H., Popp, T., Rasmussen, S. O., Raynaud, D., Rothlisberger, R., Ruth, U., Samyn, D., Schwander, J., Shoji, H., Siggard-Andersen, M.-L., Steffensen, J. P., Stocker, T. F., Sveinbjörnsdóttir, A. E., Svensson, A., Takata, M., Tison, J.-L., Thorsteinsson, T., Watanabe, O., Wilhelms, F., and White, J. W. C.: High-resolution record of Northern Hemisphere climate extending into the last interglacial period, Nature, 431, 147–151, 2004.

CPD
11, 2341–2388, 2015

Bamber, J. L., Griggs, J. A., Hurkmans, R. T. W. L., Dowdeswell, J. A., Gogineni, S. P., Howat, I., Mouginot, J., Paden, J., Palmer, S., Rignot, E., and Steinhage, D.: A new bed elevation dataset for Greenland, The Cryosphere, 7, 499–510, doi:10.5194/tc-7-499-2013, 2013.

Bigler, M., Wagenbach, D., Fischer, H., Kipfstuhl, J., Millar, H., Sommer, S., and Stauffer, B.: Sulphate record from a northeast Greenland ice core over the last 1200 years based on continuous flow analysis, in: Annals of Glaciology, vol. 35, edited by: Wolff, E. W., Int. Glaciological Soc., Cambridge, 250–256, 2002.

Box, J. E.: Survey of Greenland instrumental temperature records: 1873–2001, Int. J. Climatol., 22, 1829–1847, 2002.

Box, J. E., Yang, L., Bromwich, D. H., and Bai, L.-S.: Greenland Ice Sheet surface air temperature variability: 1840–2007*, J. Climate, 22, 4029–4049, 2009.

Buchardt, S. L., Clausen, H. B., Vinther, B. M., and Dahl-Jensen, D.: Investigating the past and recent δ^{18}O-accumulation relationship seen in Greenland ice cores, Clim. Past, 8, 2053–2059, doi:10.5194/cp-8-2053-2012, 2012.

Buizert, C., Gkinis, V., Severinghaus, J. P., He, F., Lecavalier, B. S., Kindler, P., Leuenberger, M., Carlson, A. E., Vinther, B., Masson-Delmotte, V., White, J. W. C., Liu, Z., Otto-Bliesner, B., and Brook, E. J.: Greenland temperature response to climate forcing during the last deglaciation, Science, 345, 1177–1180, 2014.

Chylek, P., Dubey, M. K., and Lesins, G.: Greenland warming of 1920–1930 and 1995–2005, Geophys. Res. Lett., 33, L11707, doi:10.1029/2006GL026510, 2006.

Crowley, T. J.: Causes of climate change over the past 1000 years, Science, 289, 270–277, 2000.

Dahl-Jensen, D., Mosegaard, K., Gundestrup, N., Clow, G. D., Johnsen, S. J., Hansen, A. W., and Balling, N.: Past temperatures directly from the Greenland Ice Sheet, Science, 282, 268–271, 1998.

Dansgaard, W.: The ^{18}O-abundance in fresh water, Geochim. Cosmochim. Ac., 6, 241–260, 1954.

Dansgaard, W.: Stabble isotopes in precipitation, Tellus, 16, 436–468, 1964.

Dansgaard, W., Johnsen, S. J., and Moeller, J.: One thousand centuries of climatic record from Camp Century on the Greenland Ice Sheet, Science, 166, 377–380, 1969.

Divine, D., Isaksson, E., Martma, T., Meijer, H. A. J., Moore, J., Pohjola, V., van de Wal, R. S. W., and Godtliebsen, F.: Thousand years of winter surface air temperature variations in Sval-

CPD
11, 2341–2388, 2015

bard and northern Norway reconstructed from ice core data, Polar Res., 30, 7379, doi:10.3402/polar.v30i0.7379, 2011.
Fischer, H. and Mieding, B.: A 1,000-year ice core record of interannual to multidecadal variations in atmospheric circulation over the North Atlantic, Clim. Dynam., 25, 65–74, 2005.
Fischer, H., Wagenbach, D., and Kipfstuhl, J.: Sulfate and nitrate firn concentrations on the Greenland Ice Sheet: 1. Large-scale geographical deposition changes, J. Geophys. Res., 103, 21927–21930, 1998a.
Fischer, H., Wagenbach, D., and Kipfstuhl, J.: Sulfate and nitrate firn concentrations on the Greenland Ice Sheet: 2. Temporal anthropogenic deposition changes, J. Geophys. Res.-Atmos., 103, 21935–21942, 1998b.
Fischer, H., Werner, M., Wagenbach, D., Schwager, M., Thorsteinnson, T., Wilhelms, F., Kipfstuhl, J., and Sommer, S.: Little Ice Age clearly recorded in northern Greenland ice cores, Geophys. Res. Lett., 25, 1749–1752, 1998c.
Fisher, D. A., Reeh, N., and Clausen, H. B.: Stratigraphic noise in time series derived from ice cores, Ann. Glaciol, 7, 76–83, 1985.
Freitag, J., Kipfstuhl, S., and Laepple, T.: Core-scale radioscopic imaging: a new method reveals density and calcium link in Antarctic firn, J. Glaciol., 59, 1009–1014, 2013.
Friedmann, A., Moore, J. C., Thorsteinnson, T., Kipfstuhl, J., and Fischer, H.: A 1200 year record of accumulation from northern Greenland, Ann. Glaciol, 21, 19–25, 1995.
Gao, C., Robock, A., and Ammann, C.: Volcanic forcing of climate over the past 1500 years: an improved ice core-based index for climate models, J. Geophys. Res.-Atmos., 113, D23111, doi:10.1029/2008JD010239, 2008.
Gray, S. T., Graumlich, L. J., Betancourt, J. L., and Pederson, G. T.: A tree-ring based reconstruction of the Atlantic Multidecadal Oscillation since 1567 A.D., Geophys. Res. Lett., 31, L12205, doi:10.1029/2004GL019932, 2004.
Grootes, P. M. and Stuiver, M.: Oxygen 18/16 variability in Greenland snow and ice with 10^{-3}- to 10^{-5}-year time resolution, J. Geophys. Res. Oceans, 102, 26455–26470, 1997.
Grootes, P. M., Stuiver, M., White, J. W. C., Johnsen, S., and Jouzel, J.: Comparison of oxygen isotope records from the GISP2 and GRIP Greenland ice cores, Nature, 366, 552–554, 1993.
Hanna, E., Jónsson, T., and Box, J. E.: An analysis of Icelandic climate since the nineteenth century, Int. J. Climatol., 24, 1193–1210, 2004.

CPD
11, 2341–2388, 2015

Isaksson, E., Kohler, J., Pohjola, V., Moore, J. C., Igarashi, M., Karlöf, L., Martma, T., Meijer, H. A. J., Motoyama, H., Vaikmäe, R., and Van de Wal, R. S. W.: Two ice-core $\delta^{18}0$ records from Svalbard illustrating climate and sea-ice variability over the last 400 years, Holocene, 15, 501–509, 2005.

Johnsen, S. J., Dansgaard, W., and White, J. W. C.: The origin of Arctic precipitation under present and glacial conditions, Tellus B, 41, 452–468, 1989.

Johnsen, S. J., Hammer, C. U., Dansgaard, W., Gundestrup, N. S., and Clausen, H. B.: The Eem stable isotpe record along the GRIP ice core and its interpreation, Quaternary Res., 42, 117–124, 1995.

Johnsen, S. J., Clausen, H. B., Cuffey, K. M., Hoffmann, G., Schwander, J., and Creyts, T.: Diffusion of stable isotopes in polar firn and ice: the isotope effect in firn diffusion, in: Physics of Ice Core Records, Hokkaido University, Place Hokkaido, 121–140, 2000.

Jónsson, T.: The Observations of Jon Thorsteinsson in Nes and Reykjavik 1820–1854, Icel. Met. Office Report, Reykjavik, 1989.

Jouzel, J., Alley, R. B., Cuffey, K. M., Dansgaard, W., Grootes, P., Hoffmann, G., Johnsen, S. J., Koster, R. D., Peel, D., Shuman, C. A., Stievenard, M., Stuiver, M., and White, J.: Validity of the temperature reconstruction from water isotopes in ice cores, J. Geophys. Res.-Oceans, 102, 26471–26487, 1997a.

Jouzel, J., Froehlich, K., and Schotterer, U.: Deuterium and oxygen-18 in present-day precipitation: data and modelling, Hydrogeological Science, 42, 747–763, 1997b.

Kinnard, C., Zdanowicz, C. M., Fisher, D. A., Isaksson, E., de Vernal, A., and Thompson, L. G.: Reconstructed changes in Arctic sea ice over the past 1,450 years, Nature, 479, 509–512, 2011.

Mann, M. E., Zhang, Z., Rutherford, S., Bradley, R. S., Hughes, M. K., Shindell, D., Ammann, C., Faluvegi, G., and Ni, F.: Global signatures and dynamical origins of the Little Ice Age and Medieval Climate Anomaly, Science, 326, 1256–1260, 2009.

Masson-Delmotte, V., Steen-Larsen, H. C., Ortega, P., Swingedouw, D., Popp, T., Vinther, B. M., Oerter, H., Sveinbjornsdottir, A. E., Gudlaugsdottir, H., Box, J. E., Falourd, S., Fettweis, X., Gallée, H., Garnier, E., Jouzel, J., Landais, A., Minster, B., Paradis, N., Orsi, A., Risi, C., Werner, M., and White, J. W. C.: Recent changes in north-west Greenland climate documented by NEEM shallow ice core data and simulations, and implications for past temperature reconstructions, The Cryosphere Discuss., 9, 655–717, doi:10.5194/tcd-9-655-2015, 2015.

CPD
11, 2341–2388, 2015

Mieding, B.: Reconstruction of Millenial Aerosol-Chemical Ice Core Records from the Northeast Greenland: Quantification of Temporal Changes in Atmospheric Circulation, Emission and Deposition, Alfred Wegener Institute for Polar and Marine Research, Bremerhaven, 2005.
Miller, G. H., Geirsdóttir, Á., Zhong, Y., Larsen, D. J., Otto-Bliesner, B. L., Holland, M. M., Bailey, D. A., Refsnider, K. A., Lehman, S. J., Southon, J. R., Anderson, C., Björnsson, H., and Thordarson, T.: Abrupt onset of the Little Ice Age triggered by volcanism and sustained by sea-ice/ocean feedbacks, Geophys. Res. Lett., 39, L02708, doi:10.1029/2011GL050168, 2012.
Newhall, C. G. and Self, S.: The volcanic explosivity index (VEI) an estimate of explosive magnitude for historical volcanism, J. Geophys. Res.-Oceans, 87, 1231–1238, 1982.
Ohmura, A.: New temperature distribution maps for Greenland, Zeitschrift für Gletscherkunde und Glaziologie, 35, 1–20, 1987.
Opel, T., Fritzsche, D., and Meyer, H.: Eurasian Arctic climate over the past millennium as recorded in the Akademii Nauk ice core (Severnaya Zemlya), Clim. Past, 9, 2379–2389, doi:10.5194/cp-9-2379-2013, 2013.
Ortega, P., Swingedouw, D., Masson-Delmotte, V., Risi, C., Vinther, B., Yiou, P., Vautard, R., and Yoshimura, K.: Characterizing atmospheric circulation signals in Greenland ice cores: insights from a weather regime approach, Clim. Dynam., 43, 2585–2605, 2014.
Pages2k Consortium: Continental-scale temperature variability during the past two millennia, Nat. Geosci., 6, 339–346, 2013.
Robock, A.: Volcanic eruptions and climate, Rev. Geophys., 38, 191–219, 2000.
Robock, A. and Mao, J.: The volcanic signal in surface temperature observations, J. Climate, 8, 1086–1103, 1995.
Schwager, M.: Ice Core Analysis on the Spatial and Temporal Variability of Temperature and Precipitation During the Late Holocene in North Greenland, Alfred Wegener Institute for Polar and Marine Research, Bremen, 2000.
Semenov, V. A. and Latif, M.: The early twentieth century warming and winter Arctic sea ice, The Cryosphere, 6, 1231–1237, doi:10.5194/tc-6-1231-2012, 2012.
Severinghaus, J. P., Sowers, T., Brook, E. J., Alley, R. B., and Bender, M. L.: Timing of abrupt climate change at the end of the Younger Dryas interval from thermally fractionated gases in polar ice, Nature, 391, 141–146, 1998.
Sigl, M., McConnell, J. R., Layman, L., Maselli, O., McGwire, K., Pasteris, D., Dahl-Jensen, D., Steffensen, J. P., Vinther, B., Edwards, R., Mulvaney, R., and Kipfstuhl, S.: A new bipolar ice

CPD
11, 2341–2388, 2015

core record of volcanism from WAIS Divide and NEEM and implications for climate forcing of the last 2000 years, J. Geophys. Res.-Atmos., 118, 1151–1169, 2013.

Sime, L. C., Risi, C., Tindall, J. C., Sjolte, J., Wolff, E. W., Masson-Delmotte, V., and Capron, E.: Warm climate isotopic simulations: what do we learn about interglacial signals in Greenland ice cores?, Quaternary Sci. Rev., 67, 59–80, 2013.

Steen-Larsen, H. C., Masson-Delmotte, V., Sjolte, J., Johnsen, S. J., Vinther, B. M., Bréon, F. M., Clausen, H. B., Dahl-Jensen, D., Falourd, S., Fettweis, X., Gallée, H., Jouzel, J., Kageyama, M., Lerche, H., Minster, B., Picard, G., Punge, H. J., Risi, C., Salas, D., Schwander, J., Steffen, K., Sveinbjörnsdóttir, A. E., Svensson, A., and White, J.: Understanding the climatic signal in the water stable isotope records from the NEEM shallow firn/ice cores in northwest Greenland, J. Geophys. Res.-Atmos., 116, D06108, doi:10.1029/2010JD014311, 2011.

Steffensen, J. P., Andersen, K. K., Bigler, M., Clausen, H. B., Dahl-Jensen, D., Fischer, H., Goto-Azuma, K., Hansson, M., Johnsen, S. J., Jouzel, J., Masson-Delmotte, V., Popp, T., Rasmussen, S. O., Rothlisberger, R., Ruth, U., Stauffer, B., Siggaard-Andersen, M. L., Sveinbjornsdottir, A. E., Svensson, A., and White, J. W.: High-resolution Greenland ice core data show abrupt climate change happens in few years, Science, 321, 680–684, 2008.

Steinhilber, F., Beer, J., and Fröhlich, C.: Total solar irradiance during the Holocene, Geophys. Res. Lett., 36, L19704, doi:1029/2009GL040142, 2009.

Swingedouw, D., Ortega, P., Mignot, J., Guilyardi, E., Masson-Delmotte, V., Butler, P. G., Khodri, M., and Séférian, R.: Bidecadal North Atlantic ocean circulation variability controlled by timing of volcanic eruptions, Nat. Commun., 6, 6545, doi:10.1038/ncomms7545, 2015.

Vinther, B. M., Andersen, K. K., Hansen, A. W., Schmith, T., and Jones, P. D.: Improving the Gibraltar/Reykjavik NAO index, Geophys. Res. Lett., 30, 2222, doi:10.1029/2003GL018220, 2003.

Vinther, B. M., Andersen, K. K., Jones, P. D., Briffa, K. R., and Cappelen, J.: Extending Greenland temperature records into the late eighteenth century, J. Geophys. Res.-Atmos., 111, D11105, doi:10.1029/2005JD006810, 2006a.

Vinther, B. M., Clausen, H. B., Johnsen, S. J., Rasmussen, S. O., Andersen, K. K., Buchardt, S. L., Dahl-Jensen, D., Seierstad, I. K., Siggaard-Andersen, M. L., Steffensen, J. P., Svensson, A., Olsen, J., and Heinemeier, J.: A synchronized dating of three Greenland Ice Cores throughout the Holocene, J. Geophys. Res.-Atmos., 111, D13102, doi:10.1029/2005JD006921, 2006b.

CPD
11, 2341–2388, 2015

Vinther, B. M., Clausen, H. B., Fisher, D. A., Koerner, R. M., Johnsen, S. J., Andersen, K. K., Dahl-Jensen, D., Rasmussen, S. O., Steffensen, J. P., and Svensson, A. M.: Synchronizing ice cores from the Renland and Agassiz ice caps to the Greenland Ice Core Chronology, J. Geophys. Res.-Atmos., 113, D08115, doi:10.1029/2007JD009143, 2008.

Vinther, B. M., Buchardt, S. L., Clausen, H. B., Dahl-Jensen, D., Johnsen, S. J., Fisher, D. A., Koerner, R. M., Raynaud, D., Lipenkov, V., Andersen, K. K., Blunier, T., Rasmussen, S. O., Steffensen, J. P., and Svensson, A. M.: Holocene thinning of the Greenland Ice Sheet, Nature, 461, 385–388, 2009.

Vinther, B. M., Jones, P. D., Briffa, K. R., Clausen, H. B., Andersen, K. K., Dahl-Jensen, D., and Johnsen, S. J.: Climatic signals in multiple highly resolved stable isotope records from Greenland, Quaternary Sci. Rev., 29, 522–538, 2010.

Weißbach, S., Wegener, A., and Kipfstuhl, J.: Snow accumulation in North Greenland over the last millennium, in: Towards an Interdisciplinary Approach in Earth System Science, edited by: Lohmann, G., Meggers, H., Unnithan, V., Wolf-Gladrow, D., Notholt, J., and Bracher, A., Springer Earth System Science, London, 197–205, 2015.

Werner, M.: Vergleichende Studie ueber die Verteilung vulkanogener Spurenstoffdepositionen in Nord-Ost-Groenland, Diplom, Institut fuer Umweltphysik, Heidelberg, 85 pp., 1995.

White, J. W. C., Barlow, L. K., Fisher, D., Grootes, P., Jouzel, J., Johnsen, S. J., Stuiver, M., and Clausen, H.: The climate signal in the stable isotopes of snow from Summit, Greenland: results of comparisons with modern climate observations, J. Geophys. Res.-Oceans, 102, 26425–26439, 1997.

Wilhelms, F.: Leitfähigkeits- und Dichtemessung an Eisbohrkernen, Alfred Wegener Institute for Polar and Marine Research, Bremerhaven, 1996.

Wood, K. R. and Overland, J. E.: Early 20th century Arctic warming in retrospect, Int. J. Climatol., 30, 1269–1279, 2010.

Wood, K. R., Overland, J. E., Jónsson, T., and Smoliak, B. V.: Air temperature variations on the Atlantic–Arctic boundary since 1802, Geophys. Res. Lett., 37, L17708, doi:10.1029/2010GL044176, 2010.

Zielinski, G. A.: Use of paleo-records in determining variability within the volcanism–climate system, Quaternary Sci. Rev., 19, 417–438, 2000.

CPD
11, 2341–2388, 2015

Table 1. Overview of all NGT drill sites.

Core Id	Core length (m)	Elevation (m a.s.l.)	Geographic Position	
			Latitude (° N)	Longitude (° W)
B16	102.4	3040	73.94	37.63
B17	100.8	2820	75.25	37.63
B18	150.2	2508	76.62	36.40
B19	150.4	2234	78.00	36.40
B20	150.4	2147	78.83	36.50
B21	100.6	2185	80.00	41.14
B22	120.6	2242	79.34	45.91
B23	150.8	2543	78.00	44.00
B26	119.7	2598	77.25	49.22
B27	175.0	2733	76.66	46.82
B28	70.7	2733	76.66	46.82
B29	110.5	2874	76.00	43.50
B30	160.8	2947	75.00	42.00

CPD
11, 2341–2388, 2015

Table 2. Depth of volcanic horizons used for dating. The given year is the time of aerosol deposition on the Greenlandic Ice Sheet. All depths are given in meter water equivalent. If a horizon could not be clearly identified a hyphen is shown in the table. A field is empty if the horizon is deeper than the length of the ice core. The maximum uncertainty is estimated from a comparison between cores dated by annual layer counting (Mieding, 2005; Schwager, 2000) and the dating used for this study. Given is also the VEI (Newhall and Self, 1982) and the total Northern Hemisphere stratospheric sulfate aerosol injection (Gao et al., 2008) for each used volcanic eruption.

Year [AD]	Event	B16	B17	B18	B19	B20	B21	B22	B23	B26	B27	B28	B29	B30	VEI	Sulfate
1912	Katmai[a]	11.60	9.31	8.48	7.38	7.86	8.62	11.56	9.49	14.27	13.69	14.44	11.41	13.12	6	11.0
1816	Tambora[a]	24.49	20.27	18.91	16.77	17.27	19.46	26.17	21.54	31.50	31.13	31.91	25.97	29.91	7	58.7
1783	Laki[a]	29.36	24.19	22.45	19.94	20.32	23.10	31.25	25.93	37.77	37.19	38.07	31.28	35.80	4	93.0
1739	Tarumai[a]	35.52	–	26.90	24.10	24.62	–	–	–	–	–		-	43.07	5	0
1694	Hekla[b]	–	34.47	31.84	28.54	29.16	32.87	44.06	–	–	–		44.22	50.45	4	0
1666	Unknown[b]	46.22	–	34.75	31.20	32.10	35.93	48.13	–	–	–		48.50	–		0
1640	Komagatake[b]	49.90	–	37.48	33.69	34.80	–	–	–	–	–		52.36	–	4	33.8
1601	Huaynaputina[a]		44.97	41.62	–	38.70	42.95	–	48.31	69.22	68.39		58.25	65.94	4	46.1
1479	Mt. St. Helenes[b]		58.84	54.42	–	51.31	56.04	75.09	–		89.42		76.81	86.60		7.4
1259	Samalas[a]			76.60	68.03	72.86			89.35		126.10			122.10		145.8
1179	Katla[a]			–	–	80.04			98.60							0
934	Eldgia[a]			109.20	99.20											0
Max. age of core [AD]		1470	1363	874	753	775	1372	1372	1023	1505	1195	1763	1471	1242		
Max. uncertainty [a]		7		3		8	6			4			3			

[a] Sigl et al. (2013).
[b] Friedmann et al. (1995).

CPD
11, 2341–2388, 2015

Table 3. Resulting mean accumulation rates (from the surface to the deepest volcanic horizon and in brackets for their common time window (1505–1953 AD)) for each NGT drill site, the lowest and highest rate within the whole core length, the time period from surface to the deepest volcanic horizon and the age at the bottom of the ice core calculated by extrapolation of the deepest calculated accumulation rate.

Core	Mean accumulation rate [kg m^{-2} a^{-1}]	Accumulation rate range [kg m^{-2} a^{-1}]	Time period [AD]	Age at bottom of core [AD]
B16	141 (141)	134–148	1640–1993	1470
B17	114 (114)	113–119	1479–1993	1363
B18	103 (106)	100–110	934–1993	874
B19	94 (94)	90–99	934–1993	753
B20	98 (100)	90–105	1179–1994	775
B21	109 (109)	105–113	1479–1994	1372
B22	145 (145)	141–154	1479–1994	1372
B23	121 (122)	116–132	1179–1994	1023
B26	176 (176)	172–190	1601–1995	1505
B27/B28	180 (181)	165–187	1783–1995	1195
B29	149 (150)	137–161	1479–1995	1471
B30	166 (169)	158–178	1259–1995	1242

CPD
11, 2341–2388, 2015

Table 4. Mean annual $\delta^{18}O$ values for each ice core, the range of the highest and lowest $\delta^{18}O$ values and the year they occurred as well as the standard deviation (SD) all given for their common time window (1953–1505 AD).

Core	Mean $\delta^{18}O$ [‰]	$\delta^{18}O$ range [‰]	Years [AD] of lowest-highest value	SD $\delta^{18}O$ [‰]	Time period [AD] (whole core length)
B16	−37.07	−40.64 to −33.11	1839–1937	0.99	1470–1993
B17	−37.13	−40.06 to −33.89	1835–1879	1.08	1363–1993
B18	−36.53	−41.52 to −31.75	1761–1889	1.44	874–1993
B19	−35.49	−38.97 to −31.77	1575–1826	1.32	753–1953
B20	−35.41	−39.34 to −30.69	1699–1929	1.42	775–1994
B21	−34.53	−38.29 to −30.95	1814–1871	1.29	1372–1994
B22	−34.54	−39.11 to −29.84	1921–1953	1.34	1372–1994
B23	−35.98	−42.11 to −32.23	1918–1928	1.28	1023–1994
B26	−33.86	−37.22 to −29.42	1597–1893	1.25	1505–1995
B27/B28	−34.47	−38.26 to −30.58	1566–1892	1.25	1195–1995
B29	−35.65	−39.22 to −31.59	1834–1928	1.18	1471–1995
B30	−35.46	−38.53 to −31.52	1862–1928	1.09	1242–1988
NGRIP*	−35.42	−40.12 to −30.81	1836–1928	1.24	

* Vinther et al. (2006b).

CPD
11, 2341–2388, 2015

Table 5. Correlation coefficients (r) of the stacked δ^{18}O-record.

	r annual	r seasonal		Years of overlap
Merged South (Greenland)[a]	0.51	DJF	0.47	1784–1994
		MAM	0.62	
		JJA	0.51	
		SON	0.5	
Ilulissat (Greenland)[a]	0.46	DJF	0.50	1784–1994
		MAM	0.42	
		JJA	0.36	
		SON	0.45	
Nuuk (Greenland)[a]	0.41	DJF	–	1784–1994
		MAM	0.55	
		JJA	0.47	
		SON	0.47	
Qaqortoq (Greenland)[a]	0.39	DJF	–	1784–1994
		MAM	0.50	
		JJA	0.50	
		SON	0.36	
Stykkisholmur (Iceland)[b]	0.41	DJF	–	1830–1994
		MAM	0.36	
		JJA	0.35	
		SON	0.31	
Mean Greenland surface air temperature[c]	0.50			1840–1994
Extended instrumental temperature record[d]	0.55			1802–1994

[a] Annual and seasonal (DJF, MAM, JJA and SON) extended Greenland temperature records (Vinther et al., 2006a).
[b] North west Iceland instrumental data (Hanna et al., 2004; Jónsson, 1989).
[c] Annual mean Greenland ice sheet near-surface air temperatures from combined instrumental and model output (Box et al., 2009).
[d] Arctic temperature reconstruction (Wood et al., 2010).
All correlations are done with 5 year running means and are significant on 95 % level ($p < 0.05$).

CPD
11, 2341–2388, 2015

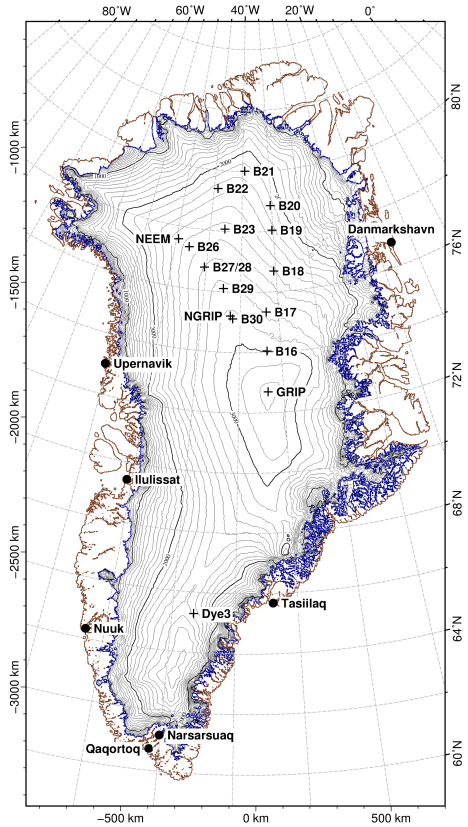

Figure 1. Map of Greenland with NGT ice cores (B16–B23, B26–B30 crosses), deep drilling sites (crosses) and towns (black dots). The ice surface topography is according to Bamber et al. (2013), (mapping: polar Stereographic (WGS84), Standard Parallel 71, Latitude of Projection Origin −39).

CPD
11, 2341–2388, 2015

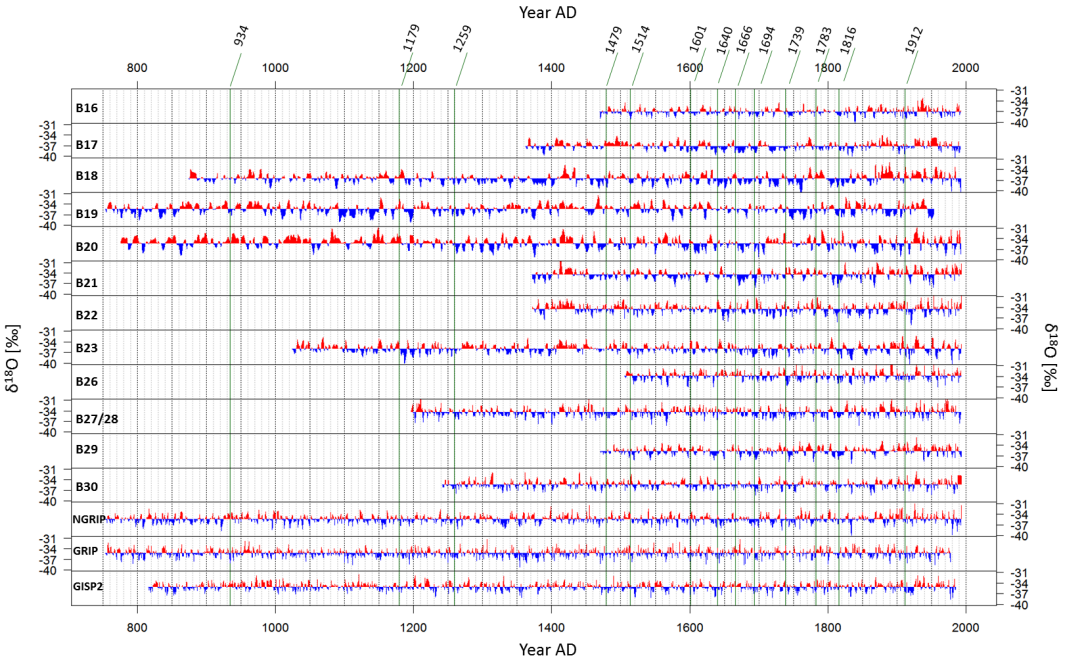

Figure 2. Annual δ^{18}O records at the 12 NGT sites (this study) and NGRIP (Vinther et al., 2006b), GRIP (Vinther et al., 2010) and GISP2 (Grootes and Stuiver, 1997). Blue are the values below the mean over their common time window (1505–1953 AD) and red are the higher ones. Dark green vertical lines mark the volcanic eruptions (years given at top) used as time markers.

CPD
11, 2341–2388, 2015

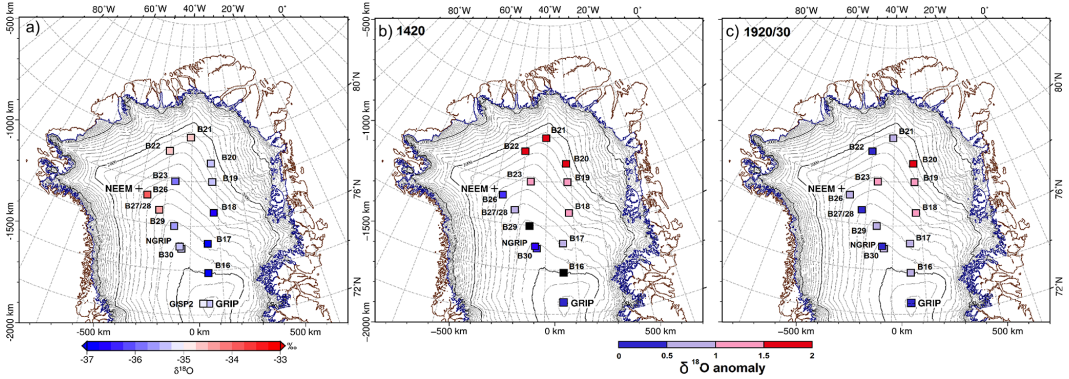

Figure 3. Spatial distribution of δ^{18}O values in northern Greenland. **(a)** The mean δ^{18}O values of the northern Greenland ice cores in their common time window (1505–1953 AD) is given with color coded squares. Blue colors representing lighter values, red colors heavier values. Mapped mean anomalies of δ^{18}O compared to **(a)** for two different periods: **(b)** 1410–1430 AD and **(c)** 1920–1940 AD. If a record not cover the required time period the square is filled in black.

CPD
11, 2341–2388, 2015

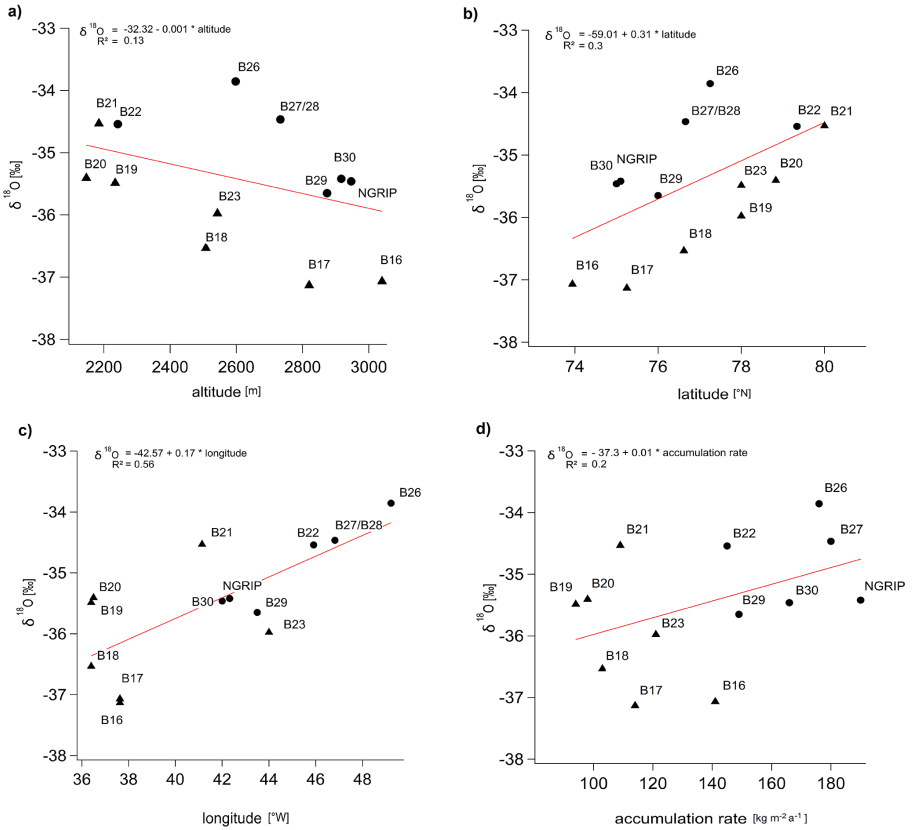

Figure 4. Mean δ^{18}O (1505–1953 AD) as a function of **(a)** altitude, **(b)** latitude and **(c)** longitude **(d)** accumulation rate of northern Greenland ice core drill sites. The red line gives the linear regression functions. Cores with higher accumulation rates ($< 145\,\mathrm{kg\,m^{-2}\,a^{-1}}$) are given as black dots and lower rates as black triangles, which is similar to the differentiation between east of and on the main ice divide.

CPD
11, 2341–2388, 2015

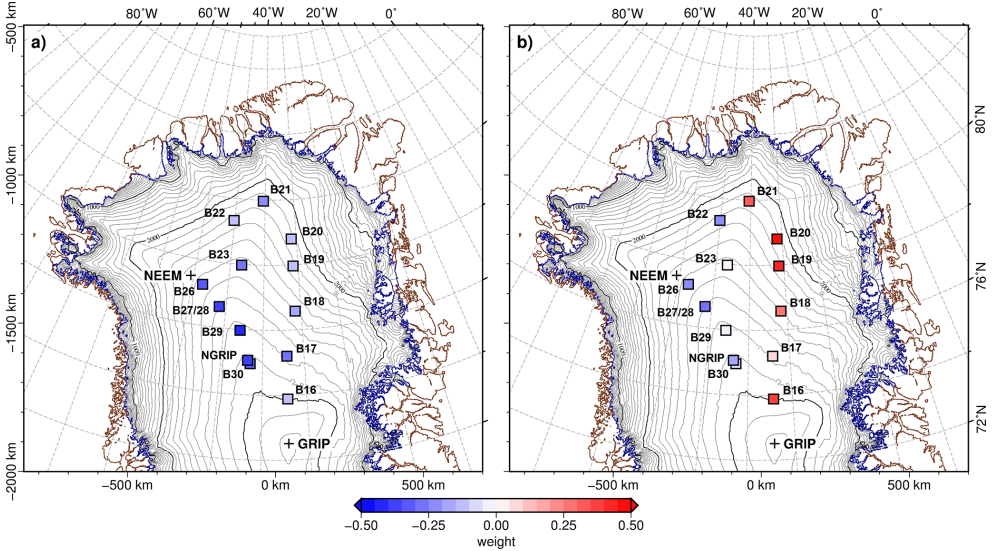

Figure 5. Map of loading for the first **(a)** and second **(b)** principal component on the annual northern Greenland $\delta^{18}O$ values between 1505 and 1953 AD.

CPD
11, 2341–2388, 2015

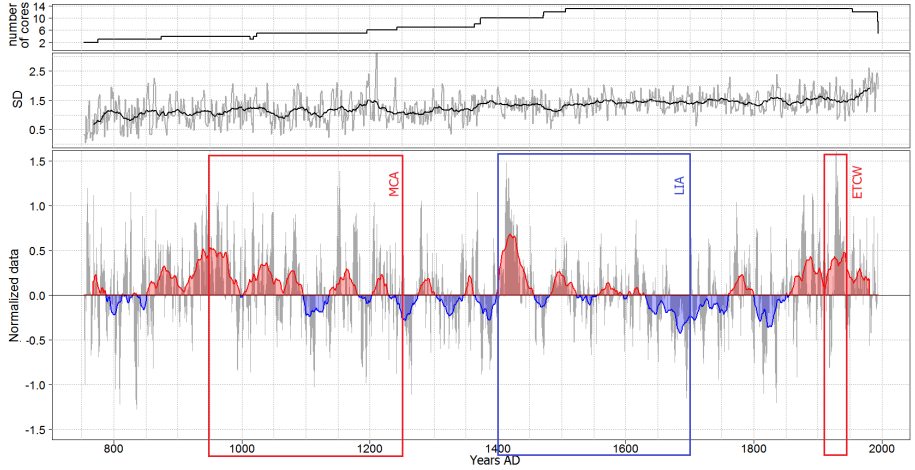

Figure 6. Annual stacked δ^{18}O (grey) and smoothed record (30 year running mean). Values more enriched compared to the mean (1953–1505 AD) are red, values less enriched are shown in blue. Known climate anomalies are marked: medieval Climate Anomaly (MCA, 950–1250 AD, Mann et al., 2009), the Little Ice Age (LIA, 1400–1700 AD, Mann et al., 2009), Early Twentieth Century Warming (ETCW, 1920–1940) (Semenov and Latif, 2012; Wood and Overland, 2010). At top of the figure the standard deviation (SD, gray: annual values, black: 30 year running mean) of all times and the number of cores used for the stack is given.

CPD
11, 2341–2388, 2015

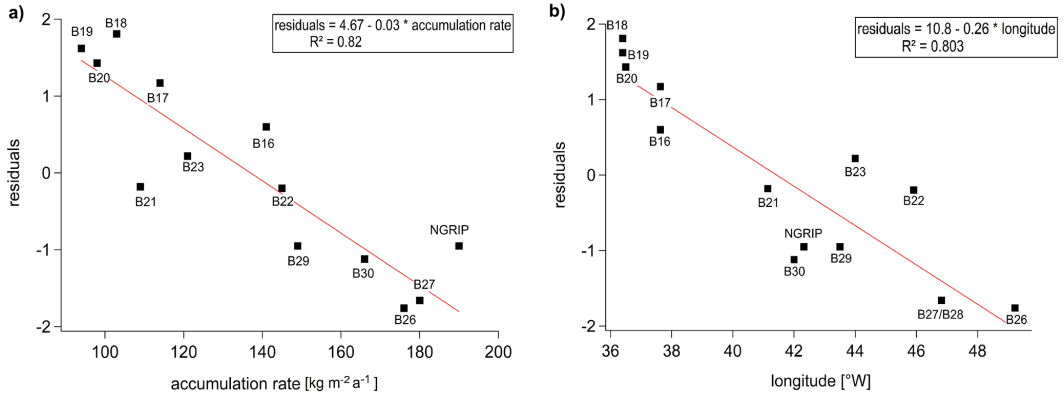

Figure 7. Residuals of the observed $\delta^{18}O$ mean values and the results of the Jonhsen model (Johnsen et al., 1989), taking into account multi parameter relationships over **(a)** the accumulation rate, **(b)** the longitude.

CPD
11, 2341–2388, 2015

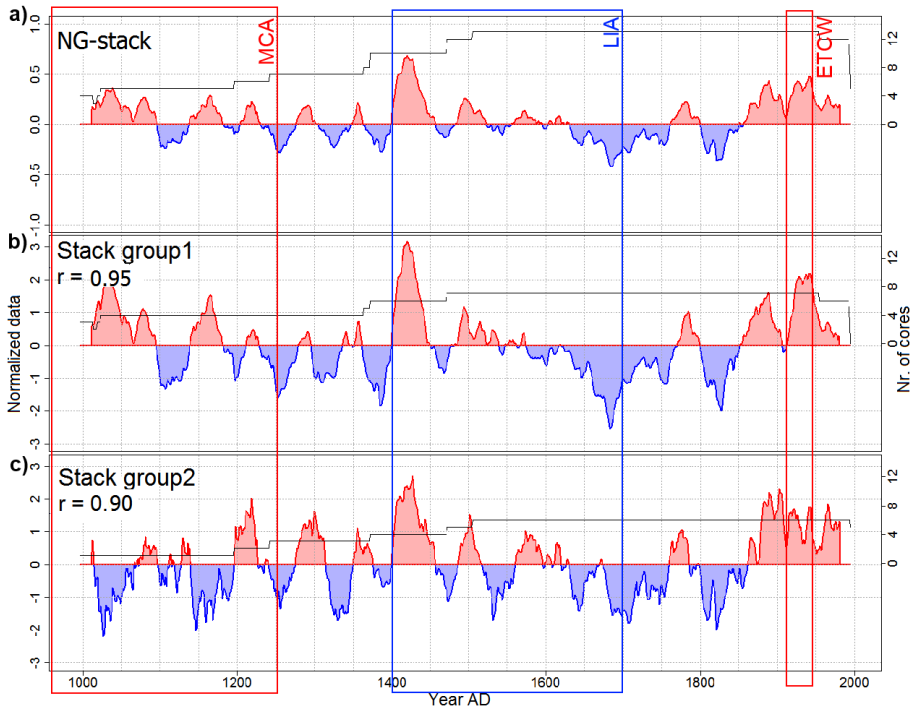

Figure 8. 30 year running mean on z levels (centred and normalized data) of stacked northern Greenland $\delta^{18}O$ records over the last 1000 years. **(a)** stack over all northern Greenland cores used in the study (NG-stack) **(b)** stack group I (B16, B17, B18, B19, B20, B21 and B23), **(c)** stack group II (B22, B26, B27, B29, B30 and NGRIP). Values in red are more enriched compared to the mean over their last 1000 years, and blue are less enriched. Given is also the correlation coefficient on 30 year running mean between the stack over all cores and the stack of the core groups (1993–1505 AD). The coefficient for a similar correlation between the two groups is calculated with $r = 0.71$.

CPD
11, 2341–2388, 2015

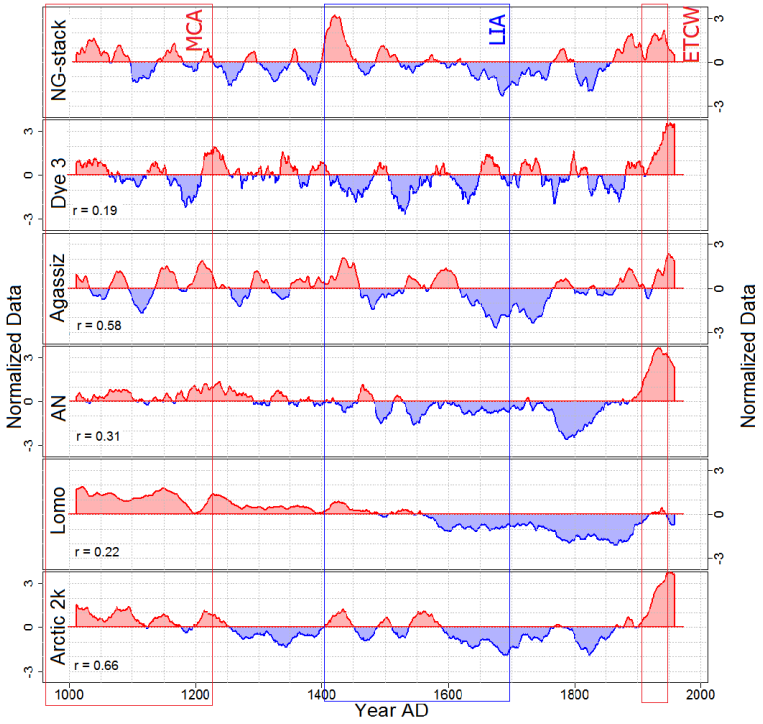

Figure 9. 30 year running mean for $\delta^{18}O$ values from different Arctic regions: northern Greenland (NG-stack, this study), southern Greenland (Dye3, Vinther et al., 2006b), Canada (Agassiz Ice Cap, Agassiz, Vinther et al., 2008), Siberia (Akademii Nauk, AN, Opel et al., 2013), Svalbard (Lomonosofvonna, Lomo, Divine et al., 2011) and a reconstructed record (Arctic2k, Pages2k Consortium, 2013). All records are given on *z* level scales (centered and normalized data). Also the correlation coefficient for the smoothed values to our stack is given.

CPD
11, 2341–2388, 2015

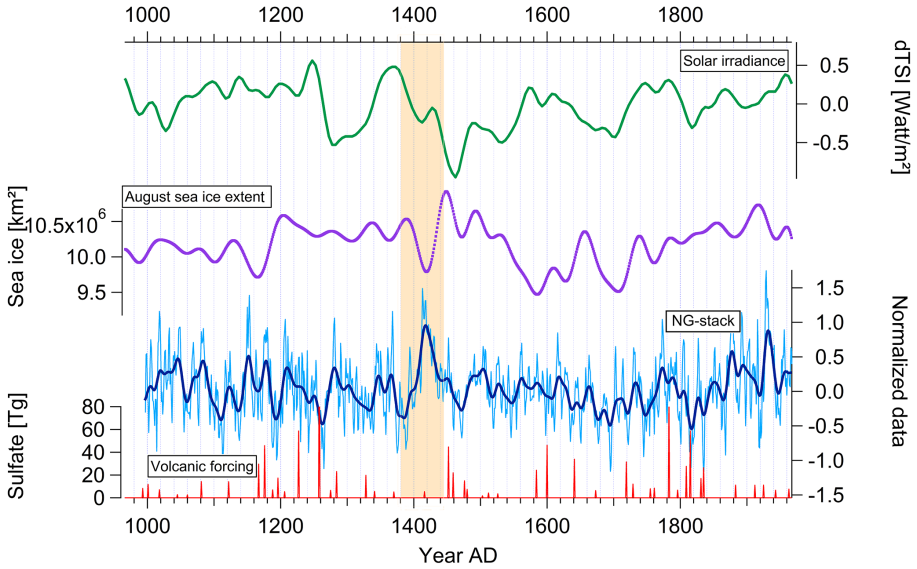

Figure 10. The northern Greenland stack (NG-stack, blue: annual, dark blue: smoothed) is shown with possible forcing factors: green the reconstructed total solar irradiance (Steinhilber et al., 2009), in purple the reconstructed August arctic sea-ice extent (Kinnard et al., 2011) and in red at the bottom the stratospheric sulphate aerosol injection for the Northern Hemisphere (Gao et al., 2008). All values are 40 year-low-pass filtered. The discussed 1420 AD event is marked with beige colour.

CPD
11, 2341–2388, 2015

Spatial and temporal oxygen isotope variability in northern Greenland

S. Weißbach et al.